Cement and Concrete Research 42 (2012) 490–498

Contents lists available at SciVerse ScienceDirect

Cement and Concrete Research

journal homepage: http://ees.elsevier.com/CEMCON/default.asp

Influence of mix proportions on microstructure and gas permeability of cement pastes and mortars

A.A. Hamami [a], Ph. Turcry [b,*], A. Aït-Mokhtar [b]

[a] Université Libre de Bruxelles, BATir, 87 Av. A. Buyl 1050 Brussels, Belgium
[b] University of La Rochelle, LaSIE, Av. M. Crépeau 17042 La Rochelle Cedex 1, France

ARTICLE INFO

Article history:
Received 20 April 2011
Accepted 30 November 2011

Keywords:
Mixture proportions (A)
Microstructure (B)
Permeability (C)
Durability (C)
Limestone filler

ABSTRACT

This paper presents a study on the influence of mix proportions of cementitious materials on their transfer properties, namely porosity and gas permeability. These latter are known as durability indicators. The work is performed on a wide range of cement pastes and mortars (24 compositions). These compositions are defined by mix proportion parameters (water/cement ratio, limestone filler/cement ratio, and amount of superplasticizer and volume fraction of paste). To characterize these materials, an experimental campaign was carried out, including different types of test (water porosimetry, mercury intrusion porosimetry, desorption isotherms and gas permeability). The influence of the composition parameters on the studied durability indicators is highlighted and correlation between gas permeability and microstructural properties (total porosity and critical pore diameter) is established. Finally, a method to predict materials permeability from that of the cement paste is proposed.

1. Introduction

Performance based approach is undoubtedly one of the most promising tool to design concrete mixtures more resistant to penetration of aggressive species responsible for reinforcement corrosion [1]. It consists in ensuring concrete durability not from mix proportions required by standard (for instance, minimum binder content or maximum water binder ratio) but from actual concrete performances against environmental loads. In order to assess concrete performances, several material properties can be used as indicators [2]. Durability indicators may be specific to a particular environmental exposure, for example, the diffusion coefficient of chloride ions for structures along coastal zones [3]. Durability indicators may also be more general, such as porosity and gas permeability. Although porosity is the most used indicator, because easy to measure by water soaking, it gives only a macroscopic idea of the material microstructure. Gas permeability, a parameter governing transfer by permeation, is a durability indicator surely more accurate than porosity, because it depends on porosity, microstructure geometry and connectivity of pores [4].

In order to design concrete mixtures with respect to permeability, it is necessary to master the relationship between the mix proportions and this transfer property and microstructure. Moreover, such a data is primordial to analyze the behavior of various new concrete mixtures, for instance, self-compacting concrete (SCC), which contains high paste fraction [5], concrete with high substitution of cement by mineral addition [6] or concrete with substitution of aggregates by local [7]. The present paper focuses on the influence of mix proportions of SCC, Especially volume fraction of paste and mineral addition content. While number of studies has been published on the influence of mix proportions on chloride diffusion coefficient of vibrated concrete, [8,9], the results on gas permeability are fewer, [10,11]. Moreover, in the case of SCC, studies are often dedicated to the comparison between vibrated concrete and SCC. For instance, Boel et al. [5] found with a large experimental campaign that SCC mixtures are about 5 times less permeable than vibrated concrete mixtures.

In this context, the aim of this study is to investigate with a parametrical study the relationship between mix proportions, microstructure and gas permeability. In order to facilitate experimental investigations, the study was carried out on pastes and mortars. The studied mix parameters were: water on cement ratio (W/C), volume fraction of paste, limestone filler (LF) content and superplasticizer content. These mix parameters were chosen for the following reasons. Limestone filler is currently used as mineral addition in SCC, with LF/C ratio often equal to 0.5. Moreover, superplasticizer is also a fundamental constituent of SCC. Since the paste is the porous medium in cementitious materials (in the widely case of impermeable aggregates), the influence of its volume fraction was investigated. An experimental campaign was carried out in order to characterize the studied materials: water porosimetry, mercury porosimetry, water vapor isothermal desorption, and gas permeability. Experimental results are discussed through modeling and literature results.

* Corresponding author. Tel.: +33 5 46 51 39 47; fax: +33 5 46 45 82 41.
E-mail address: philippe.turcry@univ-lr.fr (P. Turcry).

0008-8846/$ – see front matter © 2011 Elsevier Ltd. All rights reserved.
doi:10.1016/j.cemconres.2011.11.019

2. Experimental program

2.1. Materials

The materials mixtures were prepared with Portland cement (C) of type CEMI 52.5 (European Standards EN 197–1), 0/3 mm siliceous sand (S), limestone filler (LF) containing more than 98% of $CaCO_3$ and PCP type superplasticizer (S_p). The properties of cement and limestone filler are given in Table 1 and Fig. 1.

2.2. Mixture proportions and preparation

Two types of materials were studied: pastes and mortars. The mix-proportions were varied considering: two water/cement mass ratios (W/C = 0.4 and 0.6) and two limestone filler/cement mass ratios (LF/C = 0 and 0.5). Note that LF/C = 0.5 is a value currently used for SCC mixtures. Based on these proportions, mortars were prepared by replacing a portion of paste volume by the same volume of sand. The volume fractions of paste, denoted P, were: 40%, 50%, 60% and 80%. For the mixtures with LF/C = 0.5, the superplasticizer contents S_p were 0 and 2% of cement mass. The principle of mix-proportioning is schematized in Fig. 2. Compositions and compressive strength of the studied mixtures are given in Table 2.

Hereafter, the term "cement paste" is used to denote mixtures containing only water and cement. The term "paste" is used to denote mixtures containing "water + cement + limestone filler" with or without superplasticizer. As shown in Fig. 2, the volume fraction of cement paste is denoted P′ while the fraction of paste P. The mixtures are named "XY-P" where "X" gives the paste composition ("PC" for paste with Portland cement, "LC" for paste with limestone filler without superplasticizer, "LC*" for paste with limestone filler and superplasticizer),"Y" gives the W/C ratio ("4" for W/C = 0.4 and"6" for W/C = 0.6) and "P" refers to the paste fraction (from 40% to 100%). For instance, PC4-60 designates a mortar with only Portland cement (X = PC), W/C = 0.4 (Y = 4) and paste fraction equal to 60% (P = 60).

The mixing procedure consisted first in mixing sand and binder during 30 s. Then, water and superplasticizer were added and the mixing was continued for 2 min. The so-obtained mixtures showed no visible segregation or bleeding. The workability was characterized by slump test with a 50 mm high and 100 mm in diameter cone. The slump flows are given in Table 2. For each mixture, a prismatic specimen (100 × 100 × 400 mm) was prepared. Mixtures were placed with vibration. The duration of vibration was fixed with respect to slump flow (the lowest is slump flow, the highest is duration). 24 h after manufacturing, the specimens were demolded and placed in a moist chamber at 98% RH. Three months later, the specimens are sawn and cored to obtain samples for the different tests described hereafter.

Table 1
Chemical composition and physical properties of the ordinary Portland cement used.

	Portland cement CEMI 52.5	Limestone filler
Chemical composition (%)		
$CaCO_3$	<0.10	98.00
CaO	63.38	<0.10
SiO_2	20.17	0.19
Al_2O_3	4.88	<0.10
Fe_2O_3	3.47	<0.10
MgO	1.20	0.46
SO_3	3.48	<0.10
C_3S	67.1	–
C_2S	8.7	–
C_3A	7.3	–
C_4AF	11.1	–
Physical properties		
Density (g/cm^3)	3.15	2.71
Blaine surface (cm^2/g)	4180	3510
Loss on ignition at 1100 °C	1.00%	43.70%

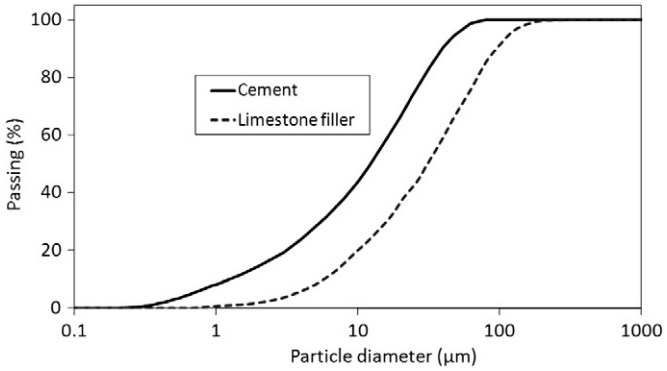

Fig. 1. Particle size distribution of cement and limestone filler obtained by laser grading.

2.3. Experimental procedures

2.3.1. Water porosity measurements

The samples for this test were disks with 64 mm diameter and from 10 mm to 16 mm thickness cored and saw-cut from the 100 × 100 × 400 mm prism. Water porosity was measured on three disks for each mixture. Water porosity measurements were carried out according to the procedure recommended by the French association AFREM [12]. Samples were first water-saturated with distilled water under vacuum at a saturation vapor pressure of 18 mmHg in order to obtain the saturated mass m_{sat}. The sample volumes V_{tot} were then determined from buoyancy weighing. Finally, samples were dried at 80 °C until mass stabilization to obtain the dried mass m_{dry}. Porosity φ was calculated using Eq. (1).

$$\varphi = \frac{V_{void}}{V_{tot}} \times 100 = \frac{m_{sat} - m_{dry}}{\rho_{water} \times V_{tot}} \times 100 \quad (\%) \tag{1}$$

Where V_{void} is the volume of the materials voids and ρ_{water} is the water density.

2.3.2. Desorption isotherm

The desorption isotherm was determined by means of a gravimetric method [13]. For each mixture, multiple crushed samples with a total mass of about 5 g were obtained from crushing of cored samples from 100x10x400 mm prism. These samples were placed at 20 ± 2 °C in sealed cells where the relative humidity RH was controlled using various saturated salt solutions or silica gel. Five RH were studied: 3%, 12%, 33%, 53.5% and 65%. For each environment, samples were regularly weighed until equilibrium was reached. It was assumed that equilibrium is reached when the hereafter criterion is satisfied: the mass loss over a 24 h period was less than 0.05%.

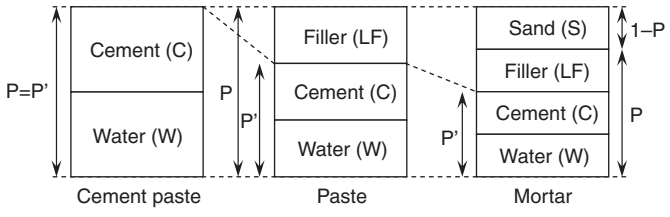

Fig. 2. Schematic view of mix proportioning method.

Table 2
Mix proportions and properties of the studied mixtures.

Mixtures	XY-P	W/C	LF/C	S_p/C	P (%)	f_{C28} (MPa)	Slump flow (mm)	Porosity (%)	K_{int} (10^{-17} m²)
PC4	PC4-40	0.4	0	0	40	60.1	154	15.4	0.27
	PC4-50				50	60.7	168	17.9	0.78
	PC4-60				60	68.4	178	20.3	1.28
	PC4-80				80	62.9	181	27.1	2.25
	PC4-100				100	57.4	183	34.0	3.74
PC6	PC6-40	0.6	0	0	40	42.2	173	18.5	2.37
	PC6-50				50	44.3	206	23.1	3.6
	PC6-60				60	42.4	211	26.8	4.23
	PC6-80				80	43.6	217	35.5	6.25
	PC6-100				100	37.7	227	43.9	7.9
LC*4	LC*4-50	0.4	0.5	0.02	50	76.5	144	16.3	7.32
	LC*4-60				60	81.2	187	19.1	0.27
	LC*4-80				80	73.3	193	23.4	0.34
	LC*4-100				100	59.9	198	28.7	1.27
LC*6	LC*6-40	0.6	0.5	0.02	40	54.4	200	15.8	1.02
	LC*6-50				50	46.3	219	18.1	1.73
	LC*6-60				60	56.1	240	21.4	3.33
	LC*6-80				80	44.7	254	30.6	3.71
	LC*6-100				100	38.8	271	36.5	5.39
LC6	LC6-40	0.6	0.5	0	40	47.8	168	17.2	1.32
	LC6-50				50	49.9	178	20.3	2.26
	LC6-60				60	53.7	197	22.9	3.12
	LC6-80				80	50.1	202	30.6	4.07
	LC6-100				100	47.2	204	37.7	5.91

The water content at equilibrium for RH, denoted w(RH), was calculated as follows:

$$w(RH) = \frac{m_{RH} - m_{dry}}{m_{dry}} \times 100 \quad (\%) \tag{2}$$

Where m_{RH} is the mass of the sample at equilibrium and m_{dry} the dried mass, obtained by oven-drying at 80 °C until the equilibrium is reached.

The water saturation degree, denoted S(RH), was also calculated:

$$S(RH) = \frac{w(RH)}{w_{sat}} \times 100 \quad (\%) \tag{3}$$

Where:

$$w_{sat} = \frac{m_{sat} - m_{dry}}{m_{dry}} \times 100 \quad (\%) \tag{4}$$

2.3.3. Mercury intrusion porosimetry (MIP)

The pore size distribution was determined from mercury intrusion on cubic samples (15×15×15 mm) from saw-cutting at mid-height of 100x100x400 prisms. The samples were first dried at a temperature of 80 °C before the test until mass stabilization. Mercury injection measurements were carried out with a Micromeritics Porosimeter (Autopore III 9420) whose range of pressure reached more than 400 MPa. This pressure range allows the mercury to penetrate pores ranging between 0.003 μm and 360 μm diameter, according to Laplace's law.

2.3.4. Gas permeability

Gas permeability was measured on cylinders 50 mm thick and 64 mm diameter, cored from the 100×100×400 mm prisms as shown in Fig. 3. These samples were then laterally surrounded by a resin to ensure radial tightness and unidirectional flow during permeability test.

Before tests, samples were slowly dried at 45 °C during 19 weeks and then dried at 80 °C until mass stabilization. These two steps are used to minimize cracking due to thermal and desiccation shrinkage gradient.

Permeability measurement was performed using a fully automatic device composed of a permeameter "Thermicar" and a data acquisition interface. The measurement principle is given by Fig. 4. The sample is placed between two chambers. The measurement proceeds in two steps. During a first step, the pressure in chamber 1 ("upstream") is increased to a high pressure (P_H > 100 kPa) and the pressure in chamber 2 ("downstream") is decreased to a low pressure (P_L ~ 8.5 kPa). The second step begins when the pressures in the two chambers are enough stabilized. Due to the pressure gradient, a gas flow occurs through the sample. The evolution of the pressure P_L in the chamber 2 is then recorded, while the high pressure P_H is maintained constant (Fig. 5). The test ends when P_L reaches 35 kPa. During this second phase, P_L has a linear evolution with time because the pressure gradient is high. An apparent permeability (K_A) expressed in m² is calculated from the slope of the curve of P_L versus time, i.e. dP_L/dt in Eq. (5):

$$K_A = \frac{2\eta L}{(P_H^2 - P_L^2)A} V_L \frac{dP_L}{dt} \tag{5}$$

Where η (Pa.s) is the dynamic viscosity of the gas, L (m) the sample thickness, V_L (m³) the volume of chamber 2 (low pressure chamber) and A (m²) the sample section.

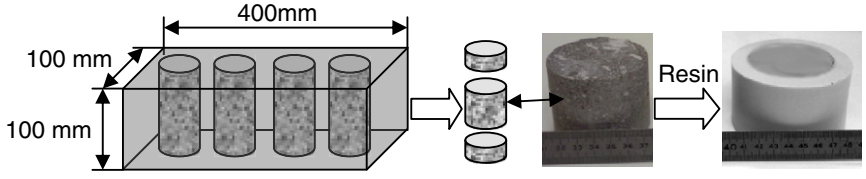

Fig. 3. Schematic view of the specimen (100×100×400 mm) and its saw-cut to obtain samples for permeability measurement.

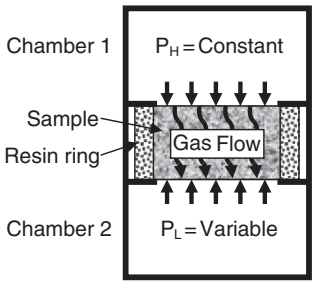

Fig. 4. Schematic view of the permeability measurement device principle.

Eq. (5) was obtained from Darcy law by assuming the gas used is ideal. Darcy law can be written:

$$Q_m = -\frac{K_A}{\eta}\frac{M}{RT}P\frac{\partial P}{\partial x}A \tag{6}$$

Where Q_m (kg/s) is the mass flux, P (Pa) is the gas pressure, T (°K) the gas temperature, M (kg/mol) the gas molar mass and R ($J.mol^{-1}.K^{-1}$) the ideal gas constant.

The mass balance in chamber 2 (downstream) can be written as follows:

$$V_L\frac{dP_L}{dt} = \frac{RT}{M}Q_m \tag{7}$$

By integrating Eq. (6) over the sample thickness and combining it with Eq. (7), we obtain the apparent permeability given by Eq. (5).

Concerning the measurements accuracy, the standard deviation is equal to approximately 20% of the measured apparent permeability values (for 3 different samples per material).

The measured permeability K_A is only an apparent permeability. K_A depends on the mean pressure P_m defined by Eq. (**8**), due to gas slippage, also called Klinkenberg effect [14,15].

$$P_m = \frac{P_H + P_L}{2} \qquad (Pa) \tag{8}$$

Thus, five tests with different high pressures (P_H = {150, 175, 200, 225, 250} kPa) were performed successively in order to assess an intrinsic permeability, denoted K_{INT}. Using the Klinkenberg method

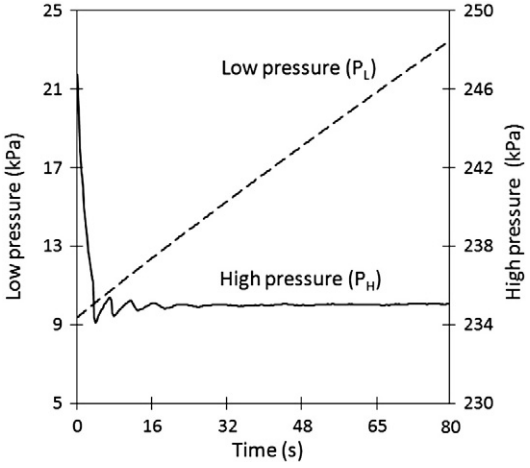

Fig. 5. Low and high pressures evolutions during permeability test.

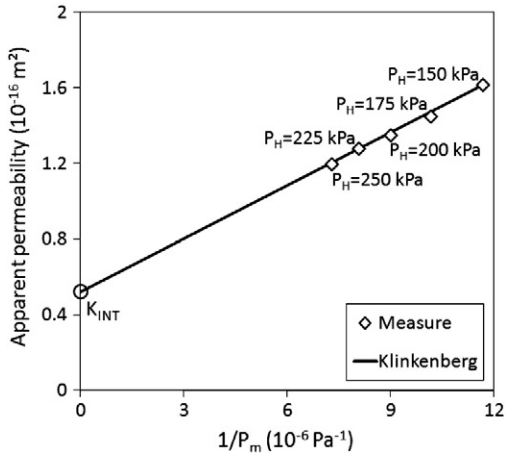

Fig. 6. Measured apparent permeability versus inverse of mean pressure — Intrinsic permeability.

[15], K_{INT} is deduced from the intercept of the curve of K_A versus 1/P_m with the y-axis (Eq. (9)):

$$K_A = K_{INT}\left(\frac{\beta}{P_m} + 1\right) \qquad (m^2) \tag{9}$$

Where β (Pa) is the Klinkenberg coefficient. An example of determination of K_{INT} is given in Fig. 6. Note that β is not a universal constant but varies with intrinsic permeability [16].

3. Results and Discussion

3.1. Water porosity

The water porosity of pastes and mortars are shown in Fig. 7. As expected, porosity increases when W/C increases for a given paste fraction [17]. The higher the W/C ratio, the higher the initial porosity to be filled by hydrates. Compared to LC mixtures (S_p/C = 0%), LC* mixtures (S_p/C = 2%) are slightly denser. Superplasticizer deflocculates cement grains to a better compaction of the powder and results in a better cement hydration [18]. The effect of superplasticizer on porosity is however small. LC mixtures (LF/C = 0.5) are less porous than PC mixtures (LF/C = 0), because their initial solid content is higher due to the limestone filler.

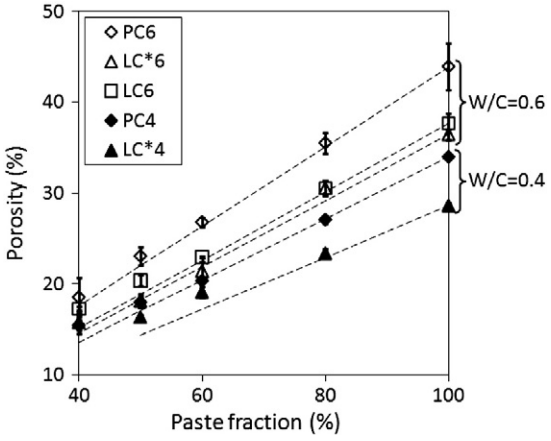

Fig. 7. Porosity versus paste fraction.

The dashed lines in Fig. 7 give porosity calculated as follows:

$$\varphi_P = P \times \varphi_{100\%} \quad (\%) \tag{10}$$

Where φ_P is the calculated porosity of the material containing a paste fraction equal to P (Fig. 2), $\varphi_{100\%}$ is the measured porosity of the paste of the corresponding mortar. It can be observed that the experimental points are almost on the so-calculated straight line. For the lower W/C ratios and lower paste fractions, the measured porosity is a little higher than the calculated one. The extra porosity may be due to a lack of compaction.

In Fig. 8, porosity is plotted versus the cement paste fraction and the dashed line corresponds to the porosity calculated as following:

$$\varphi_{p'} = P' \times \varphi_{100\%} \quad (\%) \tag{11}$$

Where P′ is the fraction of cement paste (Fig. 2). Once again, the measured porosities are close to the calculated ones (dashed lines). The observed effect of limestone filler and sand fractions on porosity is mainly a dilution effect. Besides, they have little influence on cement hydration, except at early age [19,20]. Ye et al. [21] have studied the influence of limestone filler on the hydration and microstructure of cement paste. They concluded that limestone filler does not participate in the chemical reaction of hydration. However, it acts as an accelerator during early cement hydration.

It is thus possible to assess the long term porosity of a given mixture from the porosity and the volume fraction of the cement paste. The assessment is less accurate for mortars with limestone filler, W/C = 0.4 and the lowest paste fractions. The excess of porosity, compared to the calculated one, could result from a lack of compaction (vibration duration not long enough). Especially, this concerns the mortar denoted LC*4–50, as discussed in the following section.

3.2. Desorption isotherms

Desorption isotherms are given in Fig. 9. Note that the curves were plotted with dash lines between RH = 65% and 100% because water contents at RH = 100% were deduced from water contents at saturation under vacuum (Section 2.3.1) and not directly measured.

Desorption isotherms carried out on the five pastes (materials with P = 100%) highlight that, for RH lower than about 50%, water contents are similar (Fig. 9 (a)). This result is confirmed by the literature [22]. For higher RH, water content of W/C = 0.6 mixtures are higher than water contents of W/C = 0.4 mixtures. This shows that macro-pores are larger for higher W/C ratio. Note that, as expected, the higher the porosity, the higher the water content at RH = 100% (obtained from water saturated samples).

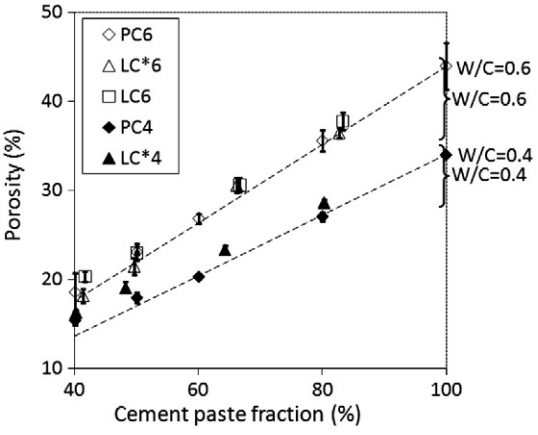

Fig. 8. Porosity versus cement paste fraction.

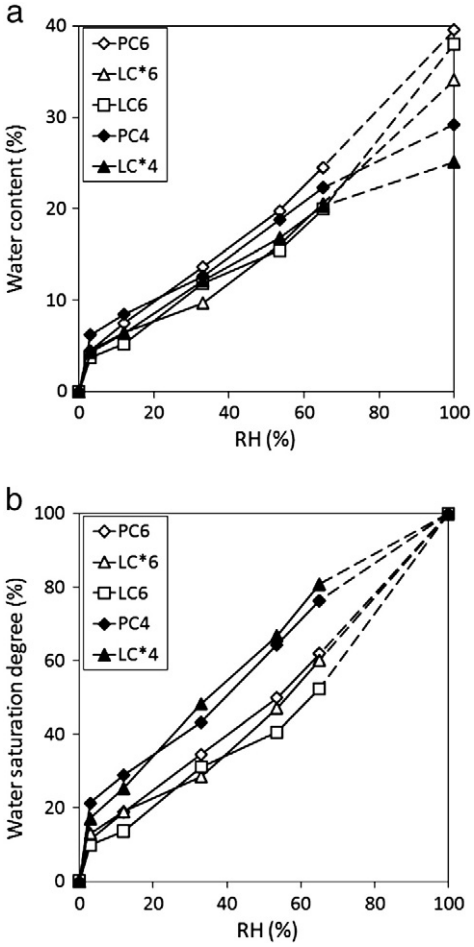

Fig. 9. Desorption isotherms of pastes (P = 100%): (a) water content at equilibrium versus RH and (b) water saturation degree at equilibrium versus RH.

In Fig. 9 (b), the water saturation degree at equilibrium was plotted versus RH. According to Kelvin equation, a given relative humidity corresponds to a pore diameter. Isotherm desorption curve can then be used to assess the pore size distribution. For a given W/C, saturation degree curves are very close. This result is of great interest. Indeed, the microstructure of paste appears mainly affected by the W/C ratio and very little by the presence of limestone filler and superplasticizer. The small effect of the limestone filler (no "filler effect") can be explained by the fact that this filler is coarser than the cement (Fig. 1).

3.3. Pore size distribution from MIP

The mercury intrusion porosimetry tests were performed only on pastes (P = 100%) and mortars with 50% paste fraction (P = 50%). Whatever the mix proportions, one main pore mode was detected (Fig. 10). Pore modes are usually classified as follows: meso-pores (approximately located between 0.1 nm and 50 nm diameter) and macro-pores (between 50 nm and 10 μm diameter) including capillary pores which are predominant [23,24].

In order to facilitate the comparison of mixtures, single values of main macro-pore diameter were determined. With this aim, normal distributions were fitted on experimental pore distribution as shown in Fig. 11. The so-obtained main pore mode diameter, denoted D_c hereafter, is the mean value of the normal distribution fitted on the main peak (Table 3).

In Fig. 12, the W/C ratio is shown to be the main parameter affecting the main pore mode diameter. For a given paste fraction, mixtures with W/C = 0.4 have systematically smaller D_c than those of mixtures with W/C = 0.6. This results from the fact that macro-pores are vestiges of

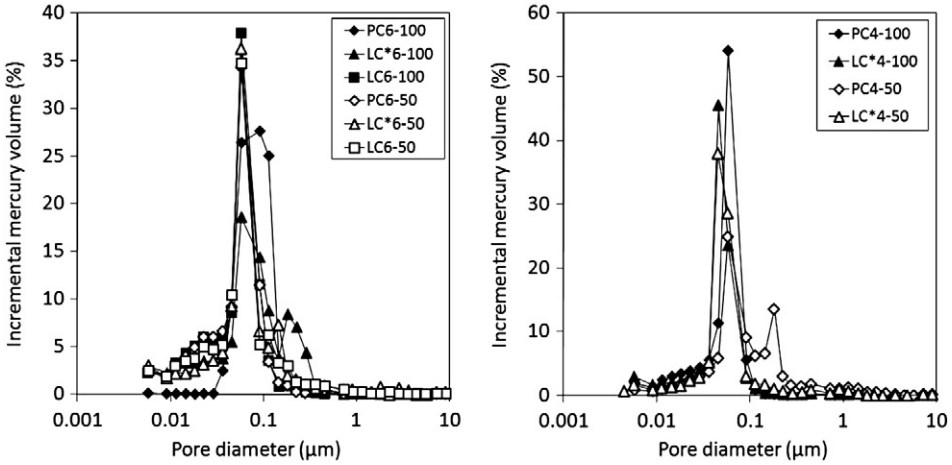

Fig. 10. Pore size distribution from MIP (left: W/C = 0.6 mixtures – right: W/C = 0.4 mixtures).

inter-granular spaces of the fresh mixture depending on the solid concentration. The effect of paste fraction is relatively small since D_c of P = 50 and 100% mixtures are almost equal. The effects of limestone filler content and superplasticizer content are also small. These effects on mix proportions on microstructure confirm those deduced from isotherm desorption.

While the effect of paste fraction on D_c is small, its effect on the overall pores distribution is more pronounced (Fig. 10). Indeed, other macro-pore modes were detected for mixtures with P = 50% (Table 3). These macro-pores are usually attributed to the interfacial transitional zone (ITZ) between aggregates and plain paste [25]. However, note that MIP detects far less these secondary pores than the critical pore mode.

As observed in the case of D_c, the effects of superplasticizer content and limestone filler on the overall pore distribution are low (Fig. 10). Only the paste denoted LC*6-100 and the corresponding mortar LC*6-50 have a secondary pore mode (Table 3). This may be the result of an interaction between superplasticizer and limestone. This effect was however not detected for W/C = 0.4.

3.4. Gas permeability

Results on gas permeability are shown in Fig. 13. As observed in the case of porosity, gas permeability increases when W/C ratio or paste fraction increases. For a given W/C ratio, the addition of limestone filler reduces gas permeability. This can be explained by the reduction in porosity when limestone filler is added. Again, the chemical effect of the admixture remains very low.

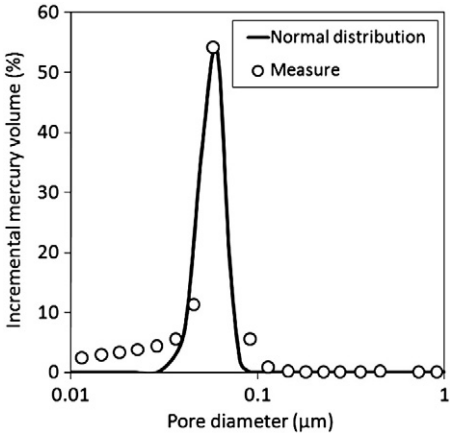

Fig. 11. Normal distribution fitted on pore size distribution from mercury intrusion (PC4-100 mixture).

The highest permeability was measured for the mixture with limestone filler and the lowest W/C and paste fraction (LC*4-50). This result is in contradiction with the above presented tendencies. The high permeability of LC*4-50 could be explained by the microstructure change due to oven-drying at 80 °C. Indeed, the microstructure of cement based material, and especially high-strength material (such as LC*4-50), are known to be damaged at temperature higher than 60 °C, because of deterioration of ettringite or CSH [26,27]. Some authors found however that the effect of temperature on microstructure is low when temperature remains lower than 105 °C [28]. Moreover, the difference in temperature effects on permeability between "normal" and high-strength materials are more often observed for temperature higher than 150 °C [29]. More probably, the high permeability of LC*4-50 could be a consequence of the lack of compaction of this mortar suspected from porosity measurements (Section 3.1). Therefore, in our opinion, this result can be considered as an experimental artifact and, at least, needs to be confirmed.

In literature, the influence of paste fraction on transfer properties is found to be sometimes low and sometimes strong. Caré [8] measured a little increase of chloride diffusion coefficient when the paste fraction decreases. Likewise, Halamickova et al. [11] observed an increase of water permeability when the paste fraction decreases. This influence of paste fraction is explained by the presence of the more porous interface between aggregates and paste, i.e. ITZ. In our case, MIP reveals few pore modes higher than the main critical mode. Moreover, as stated by Halamickova et al. [11], one parameter is often badly controlled, namely the air content, which depends strongly on the compaction procedure of the fresh material. Therefore, the observed trends should depend also of the compaction task, as revealed by the higher permeability measured for LC*4-50. In the following analyses, results for this mixture were not taken into account.

Table 3
Pore modes assessed from MIP.

Mixtures	Main pore mode D_c (nm)	Secondary pore mode (nm)
PC6-100	75	–
PC4-100	58	–
LC*6-100	70	200
LC*4-100	45	–
LC6-100	70	–
PC6-50	70	–
PC4-50	58	180
LC*6-50	60	140
LC*4-50	45	450
LC6-50	70	110

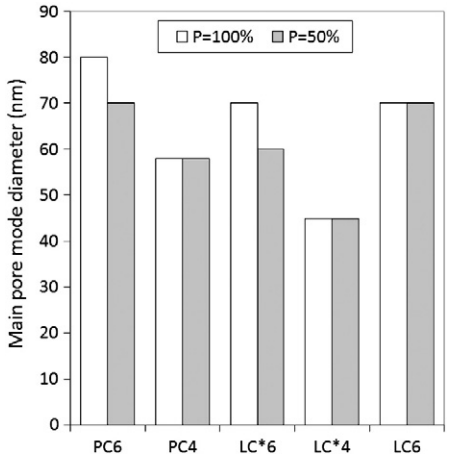

Fig. 12. Main pore mode diameter D_c deduced from MIP versus paste composition and paste fraction.

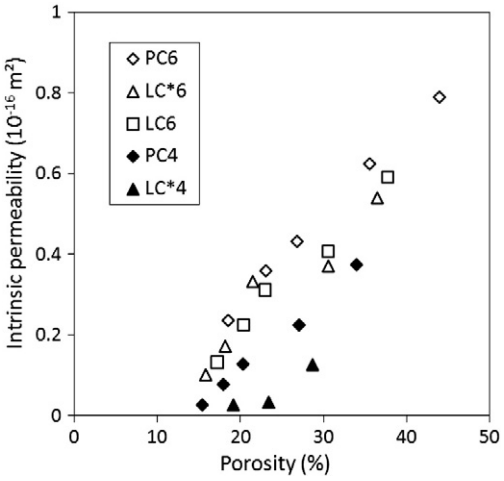

Fig. 14. Intrinsic gas permeability versus porosity.

3.5. Correlation between gas permeability, porosity and main mode pore diameter

For a given W/C ratio, correlation between permeability and porosity is roughly linear (Fig. 14). In particular, a rather good correlation is found for W/C = 0.6 mixtures. The knowledge of porosity is however not enough to predict permeability whatever the mix proportions. Indeed, for the same porosity, W/C = 0.4 mixtures are less permeable than W/C = 0.6 mixtures.

According to Poiseuille's law, permeability should depend on both open porosity and connected pores size. Especially, permeability should be proportional to the product of porosity and squared main mode pore diameter, as shown by Garboczi [30] and Katz and Thompson [31]. In literature, a number of models have been developed to predict permeability from MIP results [32–35]. For instance, Katz and Thompson proposed to determine the main pore diameter from the inflection point on the mercury intrusion curve (as done in Section 3.3) [31].

For each mixture, the measured intrinsic permeability were plotted versus $\varphi.D_c^2$, with φ the porosity and D_c the main pore mode diameter determined as explained in previous section. A good correlation is found as shown in Fig. 15. This confirms that permeability depends not only on porosity but also on pores size.

Permeability should depend also on other factors, such as connectivity and tortuosity of the microstructure. Therefore, another approach was investigated below to model mortars permeability.

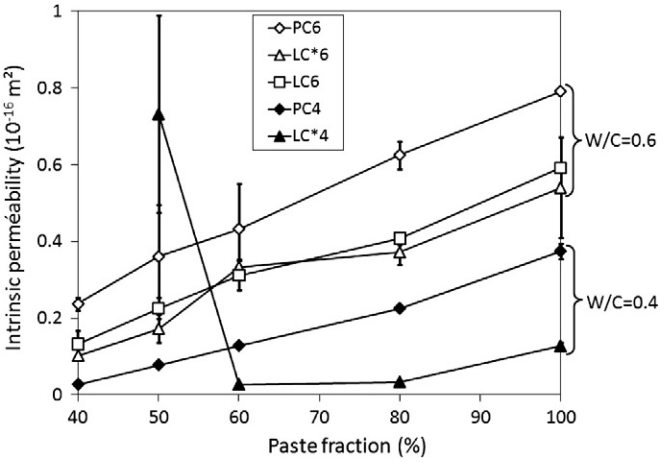

Fig. 13. Intrinsic permeability versus paste fraction.

3.6. From paste permeability to mortar permeability

In the literature, one can find several attempts to predict transfer property of concrete or mortar knowing the corresponding property of the paste, for instance chloride diffusion coefficient [8,9,36] or electrical conductivity [37]. In these approaches, concrete mixtures or mortars are considered as composites made of inclusions (aggregates) and matrix (paste). According to Caré [8], three effects on permeability due to the presence of aggregates in mortar can be distinguished.

- If sand is assumed to be impermeable compared to paste, permeability should then increase with paste fraction due to a dilution effect given by Eq. (12).

$$K_{P\%} = \frac{P}{100} K_{100\%} \quad (m^2) \tag{12}$$

Where $K_{P\%}$ is the permeability of a mortar containing a paste fraction equal to P (in%) and $K_{100\%}$ is the permeability of the paste.

- The addition of sand lengthens the path of gas flow. Both dilution and tortuosity effects can then be modeled by Eq. (13)

$$K_{P\%} = \frac{P}{100\tau} K_{100\%} \quad (m^2) \tag{13}$$

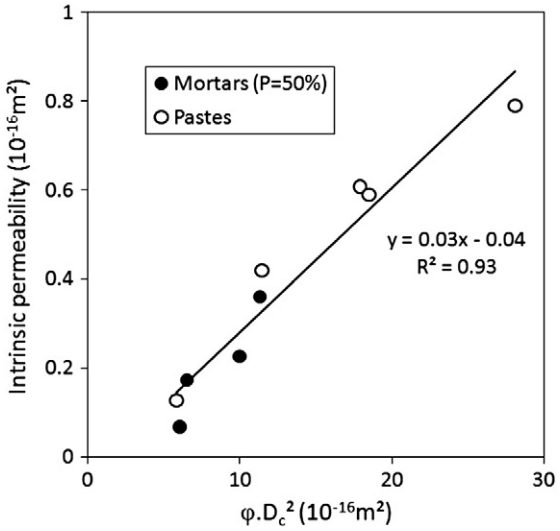

Fig. 15. Intrinsic gas permeability versus $\varphi.D_c^2$.

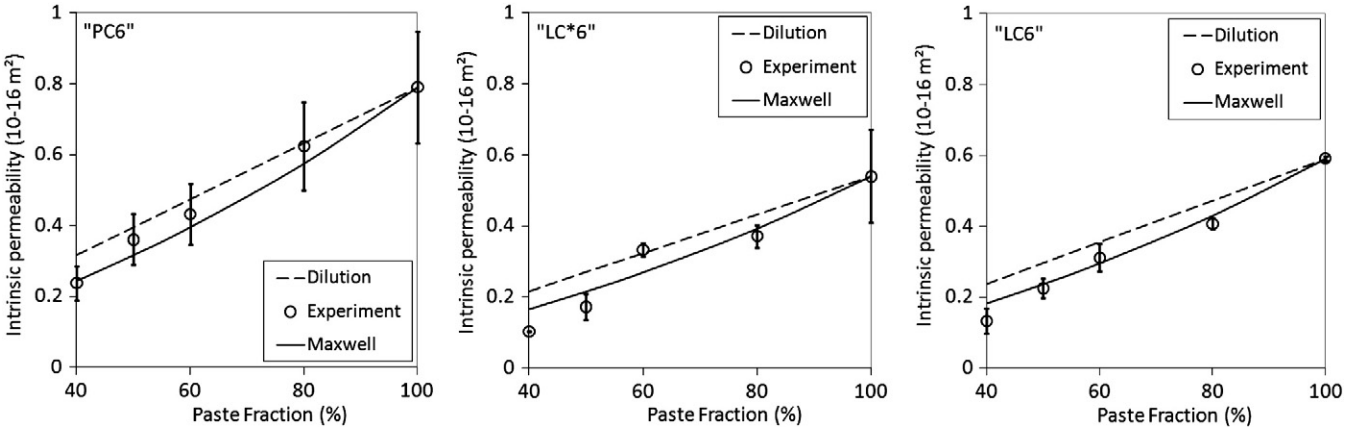

Fig. 16. Dilution and tortuosity effect on the permeability of mortars with W/C = 0.6.

where the tortuosity τ can be calculated using Maxwell's model in the case of spherical inclusions by:

$$\tau = \frac{300 - P}{200} \tag{14}$$

– The ITZ around sand grains is known to be more porous than the bulk paste. Thus, the presence of ITZ should result in an increase of permeability. This can be modeled as follows:

$$K_{p\%} = f(P_{ITZ})\left(\frac{P}{100\tau}\right)K_{100\%} \quad (m^2) \tag{15}$$

Where $f(P_{ITZ})$ is a function of the volume fraction of ITZ used to take into the increase effect due to ITZ in the Maxwell model. Caré provided an empirical expression of $f(P_{ITZ})$ in the case of chloride diffusion coefficient [8]. Note also that the volume fraction of ITZ can be assessed from the aggregates size distribution following the procedure developed by Torquato and Lu [38] and described by Garboczi and Bentz [39].

For W/C = 0.6 mixtures (Fig. 16), mortar permeabilities are well assessed from paste permeability and Maxwell model given by Eqs. (13) and (14). Thus, for these mortars, permeability is mainly affected by the combined effects of dilution and tortuosity due to inclusions. For mortars with W/C = 0.4 (Fig. 17), Maxwell's model is less efficient. This could be due to the fact that the Maxwell's model is maybe too simple to assess properly tortuosity since aggregates are modeled by mono-dispersed spherical inclusions. In both cases, measured permeabilities are equal or lower than calculated permeabilities from Maxwell's model. This tends to prove that the increase effect of permeability due to the ITZ is very small for our mortars. This confirms results of Basheer et al. [10]. These authors found that the gas permeability decreases with the increase of fine aggregate content, due to the dilution and tortuosity effects, while the ITZ is less porous in the case of finer aggregates.

4. Conclusion

We study in this paper the relationship between mix proportions, microstructure and gas permeability of cementitious materials. Based on the results, the following conclusions can be made.

- W/C ratio and paste volume fraction were found to be the main mix parameters affecting porosity and gas permeability.
- The influence of superplasticizer content (2% of the cement mass) on porosity and gas permeability was found to be very small.
- The limestone filler was found to have little effects on porosity and gas permeability, except a dilution effect such as an inert inclusion in the cement paste. Moreover, the low effect on microstructure was confirmed by both desorption isotherm and MIP tests. Indeed, the knowledge of the property (porosity or permeability) of the cement paste and its volume fraction permit to assess the same property of paste or mortars.
- For a given W/C, gas permeability is roughly correlated to porosity. However, porosity is not enough to predict permeability whatever mix proportion. One have to take into account data provided information on microstructure pore size. Indeed, permeability appears to be well correlated to porosity and the diameter of the main pore mode deduced from MIP.

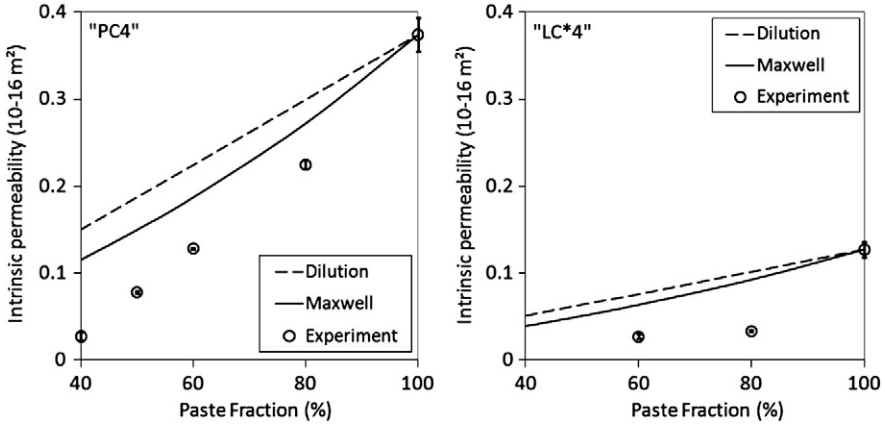

Fig. 17. Dilution and tortuosity effect on the permeability of mortars with W/C = 0.4.

- The knowledge of the properties of the cement paste (mix of cement and water) and the paste fraction appear to be enough to give relatively good prediction of the properties of mortars. However, in the case of low W/C ratios, this kind of assessment is less accurate. It is considered that the studied properties are dependent on the compaction quality of the material at the fresh state. Thus, in order to design models predicting gas permeability as a function of mix parameters, efforts have to be made also to predict air content of the mixture.

Further investigations are planned to confirm these results on concrete mixtures.

References

[1] E. Rozière, A. Loukili, F. Cussigh, A performance based approach for durability of concrete exposed to carbonation, Constr. Build. Mater. 23 (1) (2009) 190–199.
[2] V. Baroghel-Bouny, T.Q. Nguyen, P. Dangla, Assessment and prediction of RC structure service life by means of durability indicators and physical/chemical models, Cem. Concr. Compos. 31 (8) (2009) 522–534.
[3] H. Friedmann, O. Amiri, A. Aït-Mokhtar, P. Dumargue, A direct method for determining chloride diffusion coefficient by using migration test, Cem. Concr. Res. 34 (11) (2004) 1967–1973.
[4] A. Abbas, M. Carcassès, J.P. Ollivier, The importance of gas permeability in addition to the compressive strength of concrete, Mag. Concr. Res. 52 (1) (2000) 1–6.
[5] V. Boel, K. Audenaert, G. De Schutter, Gas permeability and capillary porosity of self-compacting concrete, Mater. Struct. 41 (7) (2008) 1283–1290.
[6] M.I.A. Khokhar, E. Roziere, P. Turcry, F. Grondin, A. Loukili, Mix design of concrete with high content of mineral additions: optimization to improve early age strength, Cem. Concr. Compos. 32 (5) (2010) 377–385.
[7] Y. Benachour, C.A. Davy, F. Skoczylas, H. Houari, Effect of a high calcite filler addition upon microstructural, mechanical, shrinkage and transport properties of a mortar, Cem. Concr. Res. 38 (6) (2008) 727–736.
[8] S. Caré, Influence of aggregate on chloride diffusion coefficient into mortar, Cem. Concr. Res. 33 (7) (2003) 1021–1028.
[9] C.C. Yang, S.W. Cho, Influence of aggregate content on the migration coefficient of concrete materials using electrochemical method, Mater. Chem. Phys. 80 (3) (2003) 752–757.
[10] L. Basheer, P.A.M. Basheer, A.E. Long, Influence of coarse aggregate on the permeation, durability and the microstructure characteristics of ordinary Portland cement concrete, Constr. Build. Mater. 19 (9) (2005) 682–690.
[11] P. Halamickova, R.J. Detwiler, D.P. Bentz, E.J. Garboczi, Water permeability and chloride ion diffusion in Portland cement mortars: relationship to sand and critical pore diameter, Cem. Concr. Res. 25 (4) (1995) 790–802.
[12] AFPC-AFREM, Durabilité des bétons: Méthodes recommandées pour la mesure des grandeurs associées à la durabilité, Compte-rendu des journées technique AFPC-AFREM, Toulouse, 1997.
[13] M. Qin, R. Belarbi, A. Ait-Mokhtar, L.O. Nilsson, Nonisothermal moisture transport in hygroscopic building materials: modeling for the determination of moisture transport coefficients, Transp. Porous Media 72 (2) (2008) 255–271.
[14] F. Couture, W. Jomaa, J.-R. Puiggali, Relative permeability relations: a key factor for a drying model, Transp. Porous Media 23 (3) (1996) 303–335.
[15] L.J. Klinkenberg, The Permeability of Porous Media to Liquids and Gases, American Petroleum Institute, Drilling and Production Practice, 1941, pp. 200–213.
[16] D.R. Gardner, A.D. Jefferson, R.J. Lark, An experimental, numerical and analytical investigation of gas flow characteristics in concrete, Cem. Concr. Res. 38 (3) (2008) 360–367.
[17] H.N. Atahan, O.N. Oktar, M.A. Tasdemir, Effects of water–cement ratio and curing time on the critical pore width of hardened cement paste, Constr. Build. Mater. 23 (3) (2009) 1996–1200.
[18] E. Sakai, T. Kasuga, T. Sugiyama, K. Asaga, M. Daimon, Influence of superplasticizers on the hydration of cement and the pore structure of hardened cement, Cem. Concr. Res. 36 (11) (2006) 2049–2053.
[19] M. Bouasker, P. Mounanga, P. Turcry, A. Loukili, A. Khelidj, Chemical shrinkage of cement pastes and mortars at very early age: effect of limestone filler and granular inclusions, Cem. Concr. Compos. 30 (1) (2008) 13–22.
[20] A.-M. Poppe, G. De Schutter, Cement hydration in the presence of high filler contents, Cem. Concr. Res. 35 (12) (2005) 2290–2299.
[21] G. Ye, X. Liu, G. De Schutter, A.M. Poppe, L. Taerwe, Influence of limestone powder used as filler in SCC on hydration and microstructure of cement pastes, Cem. Concr. Compos. 29 (2) (2007) 94–102.
[22] V. Baroghel-Bouny, Water vapour sorption experiments on hardened cementitious materials: part I: essential tool for analysis of hygral behavior and its relation to pore structure, Cem. Concr. Res. 37 (3) (2007) 414–437.
[23] F. de Larrard, Construire en béton, ENPC Press, Paris, 2002.
[24] M.M.Y. Delmi, Étude de l'hydratation et du couplage carbonatation-échanges hydriques dans les mortiers et bétons. PhD Thesis of the University of La Rochelle, 2004.
[25] J.-P. Ollivier, J.-C. Maso, B. Bourdette, Interfacial transition zone, Adv. Cem. Based Mater. 2 (1) (1995) 30–38.
[26] C. Gallé, Effect of drying on cement-based materials pore structure as identified by mercury intrusion porosimetry. A comparative study between oven-, vacuum, and freeze-drying, Cem. Concr. Res. 31 (10) (2001) 1467–1477.
[27] M.A. Sanjuán, R. Muñoz-Martialay, Oven-drying as a preconditioning method for air permeability test on concrete, Mater. Lett. 27 (4–5) (1996) 263–268.
[28] A.N. Noumowé, P. Clastres, G. Debicki, J.-L. Costaz, Nucl. Eng. Des. 166 (1) (1996) 99–108.
[29] Tsimbrovska M., Dégradation des bétons à hautes performances soumis à des températures élevées. Evolution de la perméabilité en liaison avec la microstructure, PhD Thesis, University of Grenoble 1, 1998.
[30] E.J. Garboczi, Mercury porosimetry and effective networks for permeability calculations in porous materials, Powder Technol. 67 (2) (1991) 121–125.
[31] A.J. Katz, A.H. Thompson, Quantitative prediction of permeability in porous rock, Phys. Rev. B 34 (11) (1986) 8179–8181.
[32] J. Kozeny, Über kapillare Leitung des Wassers im Boden. Sitzungsber. Academy of Science of Vienna 136 (1927) 271–306. In O. Bonnefoy PhD Thesis, École Nationale Supérieure des Mines de St Etienne, 2005.
[33] E.J. Garboczi, Permeability, diffusivity and microstructural parameters: a critical review, Cem. Concr. Res. 20 (4) (1990) 591–601.
[34] A. Aït-Mokhtar, O. Amiri, P. Dumargue, S. Sammartino, A new model to calculate water permeability of cement based materials from MIP results, Adv. Cem. Res. 14 (2) (2002) 43–49.
[35] O. Amiri, A. Aït-Mokhtar, M. Sarhani, Tri-dimensional modelling of cementitious materials permeability from polymodal pore size distribution obtained by mercury intrusion porosimetry tests, Adv. Cem. Res. 17 (1) (2005) 39–45.
[36] L. Dormieux, E. Lemarchand, Modélisation macroscopique du transport diffusif – Apport des méthodes de changement d'échelle d'espace, Oil Gas Sci. Technol. – Revue de l'IFP 55 (1) (2000) 15–34.
[37] E.J. Garboczi, L.M. Schwartz, D.P. Bentz, Modelling the influence of interfacial zone on the DC electrical conductivity of mortar, Adv. Cem. Based Mater. 2 (5) (1995) 169–181.
[38] S. Torquato, B. Lu, Nearest-surface distribution functions for polydispersed particle system, Phys. Rev. A 45 (8) (1992) 5530–5544.
[39] E.J. Garboczi, D.P. Bentz, Analytical formulas for interfacial transition zone properties, Adv. Cem. Based Mater. 6 (3–4) (1997) 99–108.